**JOURNAL OF THEORETICAL
AND APPLIED MECHANICS**
2, **39**, 2001

NUMERICAL ANALYSIS OF THICK, MULTI-LAYERED COMPOSITE GIRDERS USING HYBRID-STRESS FINITE ELEMENTS

Jerzy Gołaś

Faculty of Civil and Environment Engineering, University of Technology and Agriculture, Bydgoszcz
e-mail: tomaszj@mail.atr.bydgoszcz.pl

This paper presents an analysis of numerical solutions for multi-layer composite girders under static loading. In the algorithms of presented solutions the hybrid-stress model of the finite element method based on Reissner's modified variational functional was used. Two versions of numerical programs were developed for an N-layer finite element. The programs were tested on the example of a three-layer laminated beam of carbon fibre-reinforced epoxy composite, as well as on the example of numerical solution for a cantilevered plate. In addition, numerical examples concerning laminated glued timber beams and a retaining wall of reinforced soil were analysed.

Key words: multi-layer composite, transverse inhomogeneity, hybrid-stress finite element, numerical analysis

1. Introduction

Multi-layer composite girders are characteristic by large transverse deformability (warping) of cross section due to variable mechanical properties of individual layers. It is, therefore, necessary to take into account the effect of transverse shear in the strength analysis of these girders and, often, the influence of elongation of normal elements as well, see Lo et al. (1977), Mau et al. (1972), Pagano (1969), Pian and Chen (1982, 1983), Rikards (1988), Spilker et al. (1977), Spilker (1980). This is particularly necessary in cases of deep girders of the depth/span ratio $h/L > 0.25$. This can, however, also apply to more slender girders, in which the ratios of the corresponding moduli of elasticity are large, i.e. $E_x^i/E_x^{i+1} > 100$ (see Gołaś, 1995, 1997). Thus correct

determination of stresses and displacements in multi-layer girders becomes possible only when it is based on the strength analysis, which takes into account the effect of the transverse shear and elongation of the normal elements.

What is presented below is the algorithm, on the basis of which a statical computation program of multi-layer cylindrically bent girders was developed. This is followed by examples of actual solutions. The hybrid stress model of the finite element method, based on the modified Reissner's variational functional was used to formulate algebraic equations. Such a model was proposed and analysed by several authors, namely: Mau et al. (1972), Pian and Chen (1982, 1983), Rikards (1988), Spilker et al. (1977), Spilker (1980).

2. Formulation of the problem

The subject of the following analysis are thick, multi-layer composite girders composed of N layers of diversified stiffness, bent to a cylindrical surface in plane x, z. The stiffness of individual layers across their thickness is constant, but can vary along the girder span – in the direction of the x axis. The material of each layer is ortothropic and linear-elastic. The girder is subjected to known static loading, applied to the external surfaces $z = \pm h/2$ and mass loading inside the volume. In addition, suitable geometrical boundary conditions are imposed on the parts of girder edges.

The girder is subdivided into an arbitrary number n_e of laminar elements by cross-sections perpendicular to the longitudinal axis x. Typical laminar finite element is shown in Fig.1.

At the edges of the elements contact at $x = 0, l$ the displacement boundary conditions $\boldsymbol{u} = \widetilde{\boldsymbol{u}}$ are satisfied. The modified Reissner variational functional assumes the following form (see Spilker et al., 1977; Spilker, 1980; Rikards, 1988)

$$\begin{aligned} \Pi_{mR}(\boldsymbol{u}, \boldsymbol{\sigma}) = \sum_{n_e} \Big\{ \sum_{i=1}^{N} \Big[-\frac{1}{2} \int\limits_{V_{ni}} \boldsymbol{\sigma}^{i\top} \mathbf{S}^i \boldsymbol{\sigma}^i \, dV + \\ + \int\limits_{V_{ni}} \boldsymbol{\sigma}^{i\top} \boldsymbol{e}^i(\boldsymbol{u}^i) \, dV - \int\limits_{V_{ni}} \widetilde{\boldsymbol{f}}_i^{\top} \boldsymbol{u}^i \, dV - \int\limits_{S_{\sigma_{ni}}} \widetilde{\boldsymbol{t}}^{\top} \boldsymbol{u}^i \, dS \Big] \Big\} \end{aligned} \tag{2.1}$$

where

$\boldsymbol{\sigma}^i, \boldsymbol{e}^i, \boldsymbol{u}^i$ – stress, strain and displacement vectors, respectively

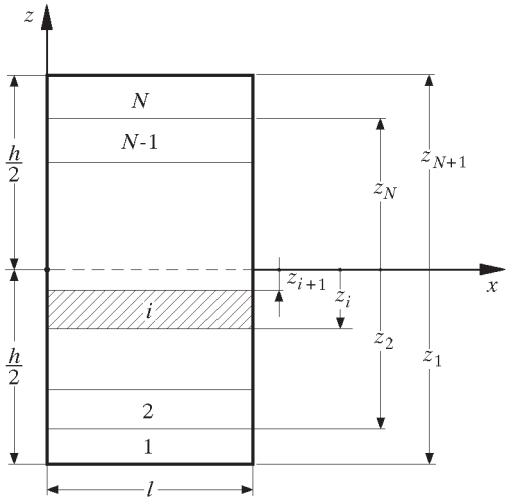

Fig. 1. Multi-layer finite element. Geometry and numeration of layers

- $\mathbf{S}^i$ – flexibility coefficient matrix of the ortothropic material in the ith layer
- V_{ni} – volume of the ith layer in nth element
- $S_{\sigma_{ni}}$ – surface on which the external loadings $\widetilde{\boldsymbol{t}}$ are imposed
- $\widetilde{\boldsymbol{f}}_i$ – mass force vector.

The stress field ${\boldsymbol{\sigma}^i}^\top = [\sigma_x^i, \sigma_z^i, \sigma_{xz}^i]$, displacement field ${\boldsymbol{u}^i}^\top = [u_i, w_i]$ and strain field ${\boldsymbol{e}^i}^\top = [\varepsilon_x^i, \varepsilon_z^i, \gamma_{xz}^i]$ are approximated by following functions (Spilker, 1980)

$$\boldsymbol{\sigma}^i = \mathbf{P}^i \begin{bmatrix} \overline{\boldsymbol{\beta}}^i \\ \boldsymbol{\beta}^i \\ \overline{\boldsymbol{\beta}}^{i+1} \end{bmatrix} = \mathbf{P}^i \boldsymbol{\beta}_i \qquad \begin{aligned} \boldsymbol{u}^i &= \mathbf{N}^i \boldsymbol{d}^i \\ \boldsymbol{e}^i &= \mathbf{B}^i \boldsymbol{d}^i \end{aligned} \tag{2.2}$$

in which $\mathbf{P}^i$, $\mathbf{N}^i$, $\mathbf{B}^i$ are appropriate matrices of the approximation functions, $\boldsymbol{d}^i$ is the nodal displacements vector and $\boldsymbol{\beta}_i$ – vector containing nodal stress parameters $\boldsymbol{\beta}^i$ assigned to the inside of a given layer, as well as the parameters $\overline{\boldsymbol{\beta}}^i$ and $\overline{\boldsymbol{\beta}}^{i+1}$ connected with its bottom and top surfaces. The stress conditions of continuity at the contact surfaces of the ith and $(i+1)$th layers

$$\sigma_z^i(z_{i+1}) = \sigma_z^{i+1}(z_{i+1}) \qquad \sigma_{xz}^i(z_{i+1}) = \sigma_{xz}^{i+1}(z_{i+1}) \tag{2.3}$$

are carried out by the equality of the corresponding parameters $\overline{\boldsymbol{\beta}}^i$ and $\overline{\boldsymbol{\beta}}^{i+1}$

of the surfaces in contact. If, at the external surfaces of the extreme layers 1 and N, the static conditions are imposed in the form

$$\sigma_{xz}^{1}(z_1) = \sigma_{z}^{1}(z_1) = 0 \qquad \sigma_{xz}^{N}(z_{N+1}) = 0 \tag{2.4}$$

then

$$\overline{\boldsymbol{\beta}}^{1} = \mathbf{0} \qquad \overline{\boldsymbol{\beta}}_{\sigma_{xz}}^{N+1} = \mathbf{0} \tag{2.5}$$

where the lower index in $(2.5)_2$ denotes the choice of these parameters $\overline{\boldsymbol{\beta}}^{N+1}$ only, which are connected with the shear stress components.

Substituting relationships (2.2) into functional (2.1), after suitable summation across all layers $i = 1, 2, ..., N$, we obtain

$$\Pi_{mc}(\boldsymbol{d}_e, \boldsymbol{\beta}) = \sum_{n_e} \Pi_{mc}^{e} = \sum_{n_e} \Big(-\frac{1}{2} \boldsymbol{\beta}^{\top} \mathbf{H} \boldsymbol{\beta} + \boldsymbol{\beta}^{\top} \mathbf{Q} \boldsymbol{d}_e - \boldsymbol{d}_e^{\top} \boldsymbol{F}_e \Big) \tag{2.6}$$

where the matrices $\mathbf{H}$, $\mathbf{Q}$ and $\boldsymbol{F}_e$ correspond to the given layered element and are appropriately composed of the following sub-matrices

$$\begin{aligned} \mathbf{H}^{i} &= \int_{V_{ni}} \mathbf{P}^{i\top} \mathbf{S}^{i} \mathbf{P}^{i} \, dV \\ \mathbf{Q}^{i} &= \int_{V_{ni}} \mathbf{P}^{i\top} \mathbf{B}^{i} \, dV \\ \mathbf{F}^{i} &= \int_{V_{ni}} \mathbf{N}^{i\top} \widetilde{\boldsymbol{f}}^{i} \, dV + \int_{S_{\sigma_{ni}}} \mathbf{N}^{i\top} \widetilde{\boldsymbol{t}}^{i} \, dS \end{aligned} \tag{2.7}$$

and the vectors $\boldsymbol{\beta}$ and $\boldsymbol{d}_e$ the components of which correspond to parameters of individual layers of the element. The nodes for the description of displacements are located only at the contacting edges of the elements $x = \text{const}$.

From the condition of stationariness of functional (2.6) with respect to the mutually independent parameters $\boldsymbol{\beta}$ and $\boldsymbol{d}_e$, we obtain

$$\boldsymbol{\beta} = \mathbf{H}^{-1} \mathbf{Q} \boldsymbol{d}_e \tag{2.8}$$

and

$$\sum_{n_e} (\mathbf{k} \boldsymbol{d}_e - \boldsymbol{F}_e) = \mathbf{0} \qquad \text{or} \qquad \mathbf{K}\mathbf{d} = \mathbf{F} \tag{2.9}$$

where

$$\mathbf{k} = \mathbf{Q}^{\top} \mathbf{H}^{-1} \mathbf{Q} \tag{2.10}$$

denotes the stiffness matrix of the layered element.

The displacements are determined from displacement algebraic equations of equilibrium (2.9) referring to the global system, following by stresses computed in individual layers of the system using relationships (2.8) and $(2.2)_1$.

Two versions of the computer program for the finite element of N layers are presented in the paper. The first having the number of stress approximation parameters $n_\beta = 14N - 5$ and the number of displacement approximation parameters $n_u = 8N + 4$, and the second $14N - 5$ and $4N + 4$, respectively.

In both versions of the program the two-dimensional stress field in each layer of the element is approximated by the relationship

$$\underbrace{\boldsymbol{\sigma}^i(x,z)}_{(3\times 1)} = \underbrace{\mathbf{P}^i(x,z)}_{(3\times 19)} \underbrace{\boldsymbol{\beta}_i}_{(19\times 1)} \tag{2.11}$$

where the polynomial functions matrix $\mathbf{P}^i(x,z)$ contains – relevantly for the components: σ_x^i – a third degree approximation in the two directions of the x and z coordinates; σ_z^i – a linear approximation in the x direction and a fifth degree approximation in the z direction; σ_{xz}^i – a quadratic approximation in the x direction and a fourth degree approximation in the z direction. For example, $P_{1,14}^i$, $P_{2,14}^i$ and $P_{3,14}^i$ elements of the $\mathbf{P}^i(x,z)$ matrix are as follows

$$P_{1,14}^i = F_i(z)x^3 \qquad P_{2,14}^i = \frac{3}{10}K_i(z)x \qquad P_{3,14}^i = \frac{3}{20}R_i(z)x^2 \tag{2.12}$$

where

$$\begin{aligned}
F_i(z) &= \frac{1}{5}(z_i^3 + 4z_i^2 z_{i+1} + 4z_i z_{i+1}^2 + z_{i+1}^3) - \frac{3}{10}(3z_i^2 + 4z_i z_{i+1} + 3z_{i+1}^2)z + z^3 \\
K_i(z) &= 2(z_i^3 z_{i+1}^2 + z_i^2 z_{i+1}^3) - z(4z_i^3 z_{i+1} + 7z_i^2 z_{i+1}^2 + 4z_i z_{i+1}^3) + \\
&+2z^2(z_i^3 + 4z_i^2 z_{i+1} + 4z_i z_{i+1}^2 + z_{i+1}^3) - z^3(3z_i^2 + 4z_i z_{i+1} + 3z_{i+1}^2) + z^5 \\
R_i(z) &= (4z_i^3 z_{i+1} + 7z_i^2 z_{i+1}^2 + 4z_i z_{i+1}^3) - 4z(z_i^3 + 4z_i^2 z_{i+1} + 4z_i z_{i+1}^2 + z_{i+1}^3) + \\
&+3z^2(3z_i^2 + 4z_i z_{i+1} + 3z_{i+1}^2) - 5z^4
\end{aligned} \tag{2.13}$$

On the other hand the parameter vector $\boldsymbol{\beta}_i$ has the form

$$\boldsymbol{\beta}_i = [\overline{\beta}_1^i, \overline{\beta}_2^i, ..., \overline{\beta}_5^i; \beta_1^i, \beta_2^i, ..., \beta_9^i; \overline{\beta}_1^{i+1}, \overline{\beta}_2^{i+1}, ..., \overline{\beta}_5^{i+1}]^\top$$

In addition, the adopted description of stresses (2.11) satisfies homogeneous equilibrium conditions in the area of the layer and static conditions on the external surfaces of the extreme layers.

In order to describe the displacement field $\boldsymbol{u}^i(x,z) = [u^i, w^i]^\top$ in a typical layer element, three nodes were assumed in the first version of the program along the edges $x = 0, l$ and two nodes in the second version. At each node two translational degrees of freedom were assumed. Thus, in each of the versions we have $n_\beta = 9$, $n_u = 12$ and $n_\beta = 9$, $n_u = 8$ independent stress parameters and displacement degrees of freedom per layer, respectively.

3. Numerical analysis and concluding remarks

The developed program was tested on the example of a three-layer plate strip considered in papers by Lo et al. (1977), Spilker (1980), Rikards (1988), bent to a cylindrical surface, for which exact analytical solutions, obtained on the basis of the theory of elasticity, are known (see Pagano, 1969). For a strip of h/L ratio equal 0.25, divided into 12 finite elements in both versions of the developed program, the relative error of the deflections reduced to dimensionless values $\overline{w}(L/2, 0)$ did not exceed 1.3%. On the other hand, the greatest deviations of the reduced values of the stress field in the cross-sections $\overline{\sigma}_x(L/2, z)$, $\overline{\sigma}_z(L/2, z)$, $\overline{\sigma}_{xz}(0, z)$ were: for the first version of the program, correspondingly 4.8, 2.1 and 8.2% – with subdivision into 12 elements, and 3.9, 1.6 and 5.6% – with subdivision into 24 elements. For the second version of the program the deviations were 5 up to 8% greater than in the first version. In view of higher precision of the solutions, further numerical analysis shall be carried out using the first version of the program.

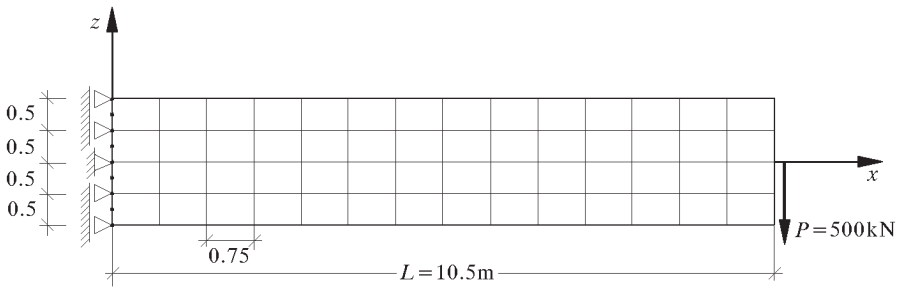

Fig. 2. Cantilever plate. Statical scheme and grid of elements

The program was also verified on the example of a FEM displacement model of cantilever plate, presented by Kleiber (1989). In this case the homogeneous cantilever plate of dimensions 2.0 m × 10.5 m, was supported on the

edge $x = 0$ and loaded by a concentrated force P at the point $(10.5, 0)$ on the free edge $x = L$ (Fig.2). The values of the vertical displacements $w(L, 0)$ at the point of application of the force P with subdivision into 10 and 14 four-layer elements differed from the solutions in Kleiber (1989) by 6.0 and 5.9%, respectively. The greatest differences in the stresses σ_x and σ_{xz} in the cross-section $x = 0.375\,\mathrm{m}$ (in order to compare the solutions of both FEM models) did not exceed 5.8%. Full picture of the obtained stress field $\boldsymbol{u}(x, z)$ and σ_x stress component are shown in Fig.3. The displacements presented there are magnified ten-fold with respect to the geometric dimensions of the plate. Intensity of shading of the surface corresponds to the increase of the stress values.

$$w_{\max} = 0.14192\,\mathrm{m};\quad u_{\max} = 0.01968\,\mathrm{m};\quad \sigma_{x_{\max}} = 7634.591\,\mathrm{kPa}$$

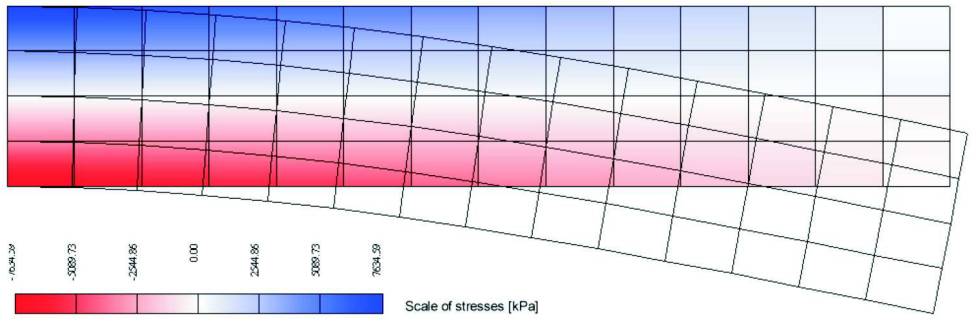

Fig. 3. Displacement field $\boldsymbol{u}(x, z)$ and normal stress component $\sigma_x(x, z)$ for isotropic cantilever plate loaded by force $P = 500\,\mathrm{kN}$ (Fig.2). Material constants: $E = 2.1 \cdot 10^6\,\mathrm{kPa},\ \nu = 0.25$

Using the developed program, bending of a glued timber laminated beam was analysed, where mechanical properties of individual layers were subjected to degradation during operation. Results of the numerical computations of the simply supported and fixed-end beam, both composed of seven layers, the properties of which changed in time from the state I to state III (according to Table 1) are presented below. The beam span was $L = 12\,\mathrm{m}$, depth $h = 1.0\,\mathrm{m}$ and the uniformly distributed load $q_z = 0.100\,\mathrm{MN/m}$ was applied to the upper surface $z = 0.5\,\mathrm{m}$. The beam was subdivided along the span into 40 laminar elements. The results of computations for beams: (a) simply supported and (b) fixed at both ends are presented in Fig.4 and Fig.5, respectively. They present the deflection of the beam axis and distribution of the normal stresses σ_x for each of the examined states I, II, and III. It was assumed that the

(a) State I

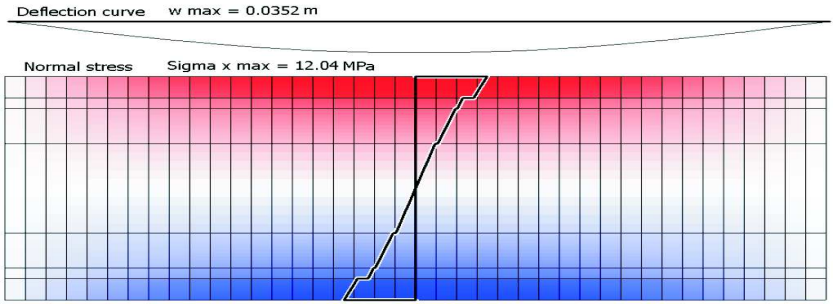

(b) State II

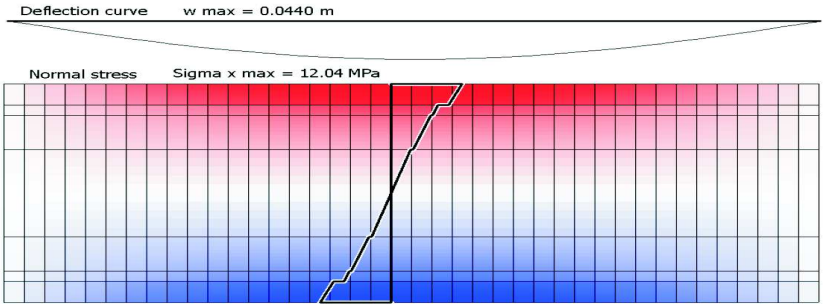

(c) State III

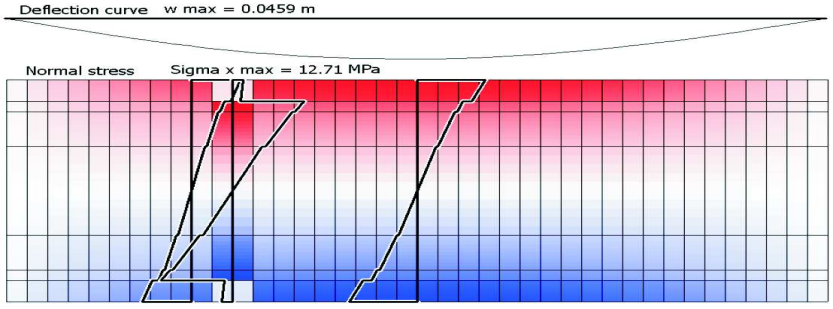

Fig. 4. Simply supported inhomogeneous beam of glued laminated wood, composed of seven layers, with stress constants changing over the operation period, according to Table 1. Deflection line of neutral axis of the beam and displacement field $\sigma_x(x, z)$ in: (a) state I, (b) state II, (c) state III – over the beam segment $3.0 \leqslant x \leqslant 3.6$ m. For the remaining length – according to state II. Note: relation between the horizontal and vertical scales is $x : z = 1 : 5$

(a) State I

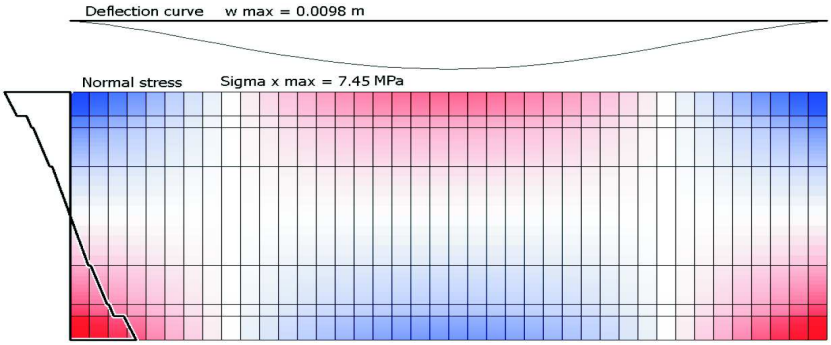

(b) State II

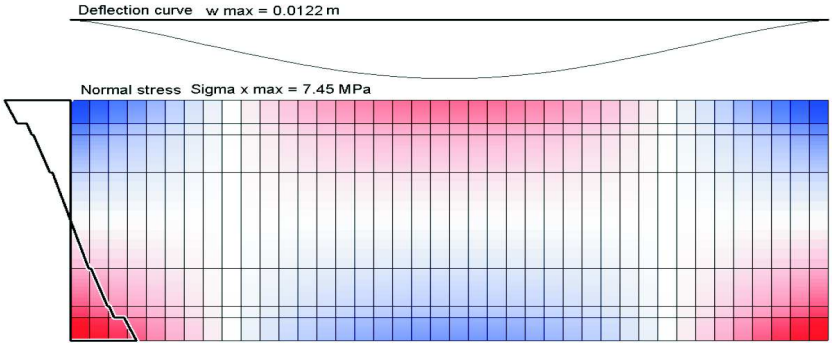

(c) State III

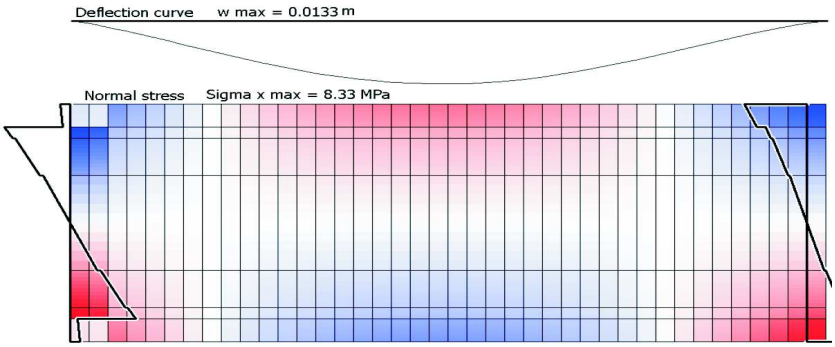

Fig. 5. Double-sided encastered beam of glued laminated wood. Description as for Fig.4, but in case (c) state III occurs over the beam segment $0 \leqslant x \leqslant 0.6\,\mathrm{m}$

state III occurs locally, i.e. between $x = 3.0\,\text{m}$ and $3.6\,\text{m}$ in beam (a) and between $x = 0$ and $0.6\,\text{m}$ in beam (b). The intensity of shading of the beam surfaces in these figures corresponds to the increase of stress. In both cases an increase of deflection and redistribution of the stress field can be noticed.

Table 1

		Material constants					
		State I		State II		State III	
Number of layer	Thickness of layer [m]	E_x [MPa]	G_{xz} [MPa]	E_x [MPa]	G_{xz} [MPa]	E_x [MPa]	G_{xz} [MPa]
1	0.096	11500	700	9200	560	920	56
2	0.048	9500	600	7600	520	7600	520
3	0.156	9000	550	7200	440	7200	440
4	0.400	8000	500	6400	400	6400	400
5	0.156	9000	550	7200	440	7200	440
6	0.048	9500	600	7600	520	7600	520
7	0.096	11500	700	9200	560	920	56

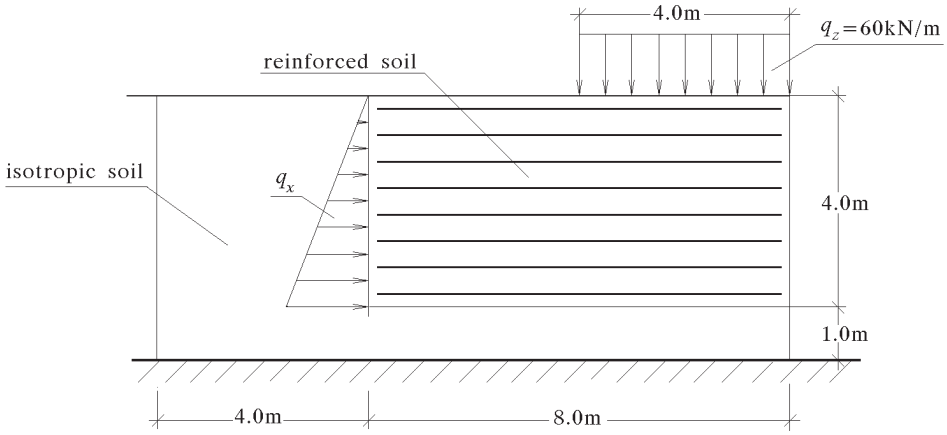

Fig. 6. Diagram of reinforced soil retaining wall structure with backfill reaction

An engineering application of the program to a statical analysis of a reinforced earth structure is given below. Theoretical bases and applications of structures of this type are presented among others by Sawicki and Kulczykowski (1986), Sawicki and Leśniewska (1993). A retaining wall of reinforced ground, loaded at its upper surface by surcharge $q_z = 60\,\text{kN/m}$ and by side

pressure of the backfill is shown in Fig.6. Own weight is also taken into account in the calculations. The structural reinforcement in the form of aluminium $0.6 \times 2.8 \times 800$ cm flat bars is placed unidirectionally in eight layers. The distance between the reinforcement in a layer is 0.5 m, the same as the distance between the layers. The following properties were assumed in the calculations:
– for the ground

$$\gamma^g = 18 \text{ kN/m}^3 \quad E^g = 1.2 \cdot 10^5 \text{ kPa}$$
$$\nu^g = 0.20 \qquad G^g = 0.5 \cdot 10^5 \text{ kPa}$$

– for the reinforcement

$$E^r = 0.72 \cdot 10^8 \text{ kPa} \qquad \nu^r = 0.34 \qquad \mu^r = 0.00067$$

where γ^α, E^α, ν^α, G^α, μ^α, denote correspondingly the bulk density, Young's modulus, Poisson's ratio, shear modulus, volumetric proportion of the component α. The technical moduli of elasticity of a single composite layer are assumed to be the following (Sawicki and Kulczykowski, 1986; Sawicki and Leśniewska, 1993)

$$E_x = 1.682 \cdot 10^5 \text{ kPa} \quad E_z = 1.215 \cdot 10^5 \text{ kPa} \qquad \nu_{zx} = 0.145$$
$$\nu_{xz} = 0.201 \qquad G_{xz} = 0.68 \cdot 10^5 \text{ kPa}$$

It was assumed in the considerations that in a block of soil, measuring $L \times h = 12.00 \times 5.00$ m zero displacement state $u = 0$, $w = 0$ occurs in the plane $z = -h/2$. The computations were carried out for two alternatives:

Alternative I: Block of soil is homogeneous and without reinforcement, loaded by surcharge q_z and own weight.

Alternative II: Retaining wall is reinforced in the above-described way, loaded by surcharge q_z, own weight and triangular backfill side load according to the formula (see Sawicki and Kulczkowski, 1986)

$$q_x = \frac{1}{2}\xi \tan^2\Big(45^\circ - \frac{\Phi}{2}\Big)\gamma h$$

where $\Phi = 37^\circ$ is the angle of internal friction of the ground, $\gamma = 18\,\text{kN/m}^3$, and $\xi = 0.618$ is the coefficient of interaction of the backfill and retaining wall.

The computed displacement state for both alternatives is presented in Fig.7 and Fig.8.

$w_{\max} = 0.00477\,\mathrm{m};\ \ u_{\max} = 0.00128\,\mathrm{m};\ \ \sigma_{z_{\max}} = 148.061\,\mathrm{kPa}$

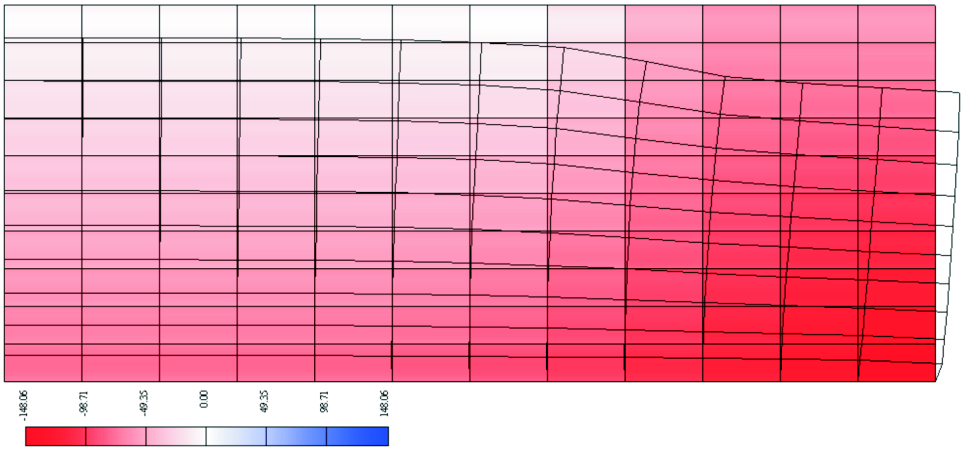

Fig. 7. Displacement field $\boldsymbol{u}(x,z)$ and distribution of stress component $\sigma_z(x,z)$ for the first loading alternative. Displacements in the diagram are 250 times enlarged with respect to dimensions of the structure

$w_{\max} = 0.00462\,\mathrm{m};\ \ u_{\max} = 0.00117\,\mathrm{m};\ \ \sigma_{z_{\max}} = 145.841\,\mathrm{kPa}$

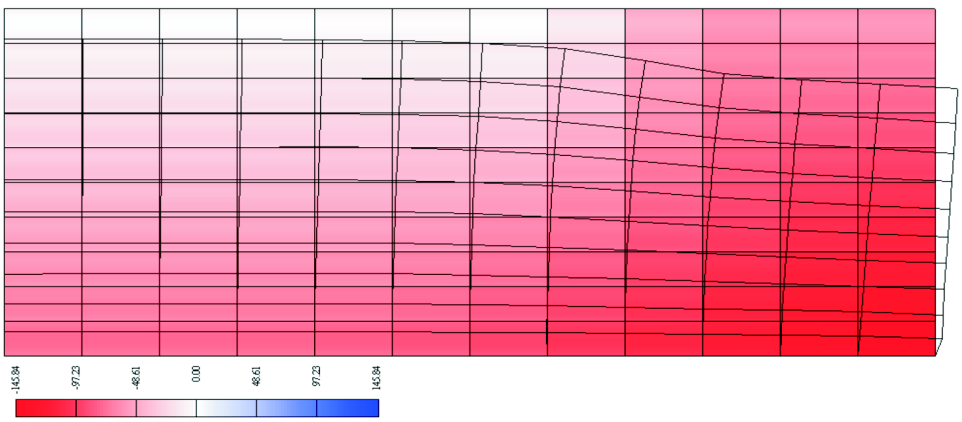

Fig. 8. Displacement field $\boldsymbol{u}(x,z)$ and distribution of stress component $\sigma_z(x,z)$ for the second loading alternative

On the grounds of the numerical analyses of the above-mentioned examples, both versions of the developed program can be recommended for determination of the displacement and stress states in thick, multi-layer ortothropic composite girders having the h/L ratio less than $1/2$. The above programs can also be used for computation of miscellaneous multi-layer engineering structures operating in a state of plane strain.

References

1. GOŁAŚ J., 1995, On Limits of Application of Kirchhoff's Hypothesis in the Theory of Viscoelastic Fibrous Composite Plates, *Engng Trans.*, **43**, 4, 603-626
2. GOŁAŚ J., 1997, On Necessity of Making Allowance for Shear Strain in Cylindrical Bending of Fibre Composite Viscoelastic Plates, *Arch. Civil Engng*, **43**, 2, 121-147
3. KLEIBER M., 1989, *Introduction to Finite Element Method* (in Polish), PWN, Warszawa-Poznań
4. LO K.H., CHRISTENSEN R.M., WU E.M., 1977, A High-Order Theory of Plate Deformation. Part 2: Laminated Plates, *J. of Applied Mechanics*, **44**, 669-676
5. MAU S.T., TONG P., PIAN T.H.H., 1972, Finite Element Solution for Laminated Thick Plates, *J. Comp. Materials*, **6**, 304-311
6. PAGANO N.J., 1969, Exact Solutions for Composite Laminates in Cylindrical Bending, *J. Comp. Materials*, **3**, 398-411
7. PIAN T.H.H., CHEN D., 1982, Alternative Ways for Formulation of Hybrid Stress Elements, *Intern. J. for Numer. Meth. in Engng*, **18**, 1679-1684
8. PIAN T.H.H., CHEN D., 1983, On the Suppression of Zero Energy Deformation Modes, *Intern. J. for Numer. Meth. in Engng*, **19**, 1741-1752
9. RIKARDS R.B., 1988, *The Finite Elements Method in Plates and Shells Theory* (in Russian), Zinatne, Riga
10. SAWICKI A., KULCZYKOWSKI M., 1986, Elastic Analysis of Reinforced – Earth Structures, *Arch. Hydrotechniki*, **33**, 3, 299-311
11. SAWICKI A., LEŚNIEWSKA D., 1993, *Reinforced Soil. Theory and Applications* (in Polish), PWN, Warszawa
12. SPILKER R.L, CHOU S.C., ORRINGER O., 1977, Alternate Hybrid-Stress Elements for Analysis of Multilayer Composite Plates, *J. Comp. Materials*, **11**, 51-70
13. SPILKER R.L., 1980, A Hybrid-Stress Finite Element Formulation for Thick Multilayer Laminates, *Computer and Structures*, **11**, 507-514

Analiza numeryczna grubych wielowarstwowych dźwigarów kompozytowych z wykorzystaniem hybrydowo-naprężeniowych elementów skończonych

Streszczenie

W pracy przedstawiono analizę rozwiązań numerycznych dla grubych wielowarstwowych dźwigarów kompozytowych obciążonych statycznie. W algorytmach rozwiązań wykorzystano hybrydowy model naprężeniowy metody elementów skończonych bazujący na zmodyfikowanym funkcjonale wariacyjnym Reissnera. Opracowano dwie wersje programu numerycznego dla elementu skończonego o N warstwach. Programy przetestowano na przykładzie trójwarstwowej belki z laminatu kompozytowego (z epoksydu wzmocnionego włóknami węglowymi) oraz na przykładzie rozwiązania numerycznego dla tarczy wspornikowej. Analizowano ponadto konkretne przykłady liczbowe dotyczące belek z drewna klejonego warstwowo oraz konstrukcji muru oporowego z gruntu zbrojonego.

Manuscript received February 24, 2000; accepted for print May 22, 2000